Local dissipation scales in two-dimensional Rayleigh-Taylor turbulence

Xiang Qiu (邱翔),[1] Yu-Lu Liu (刘宇陆),[1,2] and Quan Zhou (周全)[2,*]
[1]*School of Science, Shanghai Institute of Technology, Shanghai 200235, China*
[2]*Shanghai Institute of Applied Mathematics and Mechanics, Shanghai University, Shanghai 200072, China*
(Received 15 April 2014; revised manuscript received 7 July 2014; published 21 October 2014)

We examine the distribution of the local dissipation scale η, $Q(\eta)$, and its temporal evolution in two-dimensional (2D) Rayleigh-Taylor (RT) turbulence using direct numerical simulations at small Atwood number and unit Prandtl number. Within the self-similarity regime of the mixing zone evolution, distributions of η at small scales are found to be insensitive to the large-scale anisotropy of the system and independent of position and of the temporal evolution of the mixing zone. Our results further reveal that the present measured $Q(\eta)$ agrees with those previously observed in homogeneous isotropic turbulence and in turbulent pipe flows, at least for the smallest scales around the classical Kolmogorov dissipation scale. However, the RT case seems to show a different trend from the other two cases for large scales, which may attributed to the absence of the inertial-range intermittency for the velocity field in 2D RT turbulence.

DOI: 10.1103/PhysRevE.90.043012 PACS number(s): 47.27.−i, 47.55.P−

I. INTRODUCTION

Dissipation is an omnipresent phenomenon in fluid turbulence occurring in nature and technology. In the classical theory of three-dimensional (3D) turbulence advanced by Kolmogorov [1–4], viscous effects become significant and energy is dissipated into heat at the scale, known as the Kolmogorov dissipation scale $\eta_K = (\nu^3/\langle\epsilon(\mathbf{x},t)\rangle)^{1/4}$. Here, ν is the kinematic viscosity of the working fluid, $\epsilon(\mathbf{x},t)$ is the local turbulent kinetic energy dissipation rate, and $\langle\cdot\rangle$ denotes an ensemble average. As a mean length scale, however, η_K cannot reveal the ubiquitous intermittent nature of turbulence, such as the intense spatiotemporal bursts of the instantaneous velocity gradient field and the local energy dissipation rate field [5,6]. To translate the intense and localized turbulent events to the dissipation scale, one can define an instantaneous fluctuating dissipation scale as $\eta(\mathbf{x},t)$, by requiring that the local Reynolds number associated with eddies of size η be of order 1, i.e., $\mathrm{Re}_\eta = \eta|\delta_\eta v|/\nu \sim 1$, where $\delta_\eta v = v_i(x_i + \eta) - v_i(x_i)$ is the longitudinal velocity increment over a separation η [7,8]. This yields the local cutoff scale η, where viscous and inertial forces balance approximately with each other [9].

In the past few years, some studies have focused on the properties of probability density functions (PDF) of η, $Q(\eta)$. By assuming the Gaussian large-scale boundary condition, the analytical predictions for $Q(\eta)$ were derived first by Yakhot [7] using Mellin transform of structure functions, and then by Biferale [10] using the multifractal formalism. Experimental results obtained from Princeton University/ONR Superpipe [11] and numerical simulations of homogeneous isotropic turbulence [12] both agree well with the theoretical distributions, thus suggesting a universal behavior of the smallest-scale fluctuations around η_K. Later, Zhou and Xia [13] generalized the ideas of η into turbulent Rayleigh-Bénard convection, a paradigm for the study of buoyancy-driven turbulence. Their results confirmed that the distributions of η are indeed insensitive to turbulent intensity and large-scale inhomogeneity and anisotropy of the system. More recently, the universality of distributions of η was further examined numerically in turbulent channel flow [14] and experimentally in the strongly anisotropic flow past a backward facing step [15]. These works suggest the universality of $Q(\eta)$ in turbulent flows with respect to different large-scale turbulence production mechanisms.

In this paper, we want to push the universality of $Q(\eta)$ one step ahead by studying distributions of the local dissipation scales, η, in nonstationary turbulent flows, which are often encountered while starting or stopping a flow process. The flow at hand is two-dimensional (2D) turbulent mixing originated at the interface that separates two layers of fluids of different densities and is accelerated against the density gradients, i.e., Rayleigh-Taylor (RT) turbulence [16,17], which has many applications in atmospheric and environment physics [18], astrophysics [19,20], and technological related problems [21–23], and provides a natural framework for the study of nonstationary turbulent flows [24,25]. Cascade processes in such a system have been extensively investigated in the past decade [26–34]. Here, two considerations prompted us to restrict ourselves to the 2D simulations of RT turbulence: (i) The numerical effort required for 2D simulations is much smaller so that a superfine resolution for the sub-Kolmogorov-scale statistics becomes feasible for high Reynolds numbers; (ii) temperature becomes a fully active scalar in the 2D RT system, and thus a new type of phenomenology, i.e., a Bolgiano-Obukhov-like (BO59) scaling [35], was theoretically predicted [36,37] and numerically observed [38–40]. Indeed, results obtained by Zhou [40] revealed that buoyancy overwhelms nonlinear energy transfer at all inertial scales. This is in clear contrast to 3D cases, where temperature behaves as a passive scalar, leading to the traditional Kolmogorov-like (K41) phenomenology as those observed in homogeneous isotropic turbulence [30]. There is the attraction of studying properties of η in a turbulent system where a non-K41 phenomenology is expected. The remainder of this paper is organized as follows. Section II provides the detailed information about the numerical method adopted. The PDFs of the local dissipation scales $Q(\eta)$ are studied and discussed

*qzhou@shu.edu.cn

in Sec. III, and we summarize our findings and conclude in Sec. IV.

II. NUMERICAL METHOD

The time-dependent incompressible Oberbeck-Boussinesq equations of miscible RT turbulence in vorticity-stream function formulation, i.e.,

$$\frac{\partial \omega}{\partial t} + (\mathbf{u}\cdot\nabla)\omega = \nu\nabla^2\omega + \beta g\frac{\partial \theta}{\partial x}, \tag{1}$$

$$\nabla^2\psi = \omega, \tag{2}$$

$$u = -\frac{\partial \psi}{\partial z}, \qquad w = \frac{\partial \psi}{\partial x}, \tag{3}$$

$$\frac{\partial \theta}{\partial t} + (\mathbf{u}\cdot\nabla)\theta = \kappa\nabla^2\theta, \tag{4}$$

are solved in a 2D box of width L_x and height L_z with uniform grid spacing Δ_g. Here, $\theta(\mathbf{x},t)$ is the temperature field, proportional to the fluid density ρ via the thermal expansion coefficient β as $\rho = \rho_0[1-\beta(\theta-\theta_0)]$ (ρ_0 and θ_0 are reference values), $\mathbf{u}(\mathbf{x},t) = u\vec{x} + w\vec{z}$ the velocity field ($\vec{x}$ and $\vec{z}$ are the horizontal and vertical unit vectors, respectively), $\omega = \nabla\times\mathbf{u}$ the vorticity, ψ the stream function, g the gravitational acceleration, and κ the thermal diffusivity of the working fluid. Periodic boundary conditions for both velocity and temperature are applied to the horizontal direction, while for the top and bottom walls, no-penetration and no-slip velocity boundary conditions, which are recast in terms of ψ as $\psi|_{z=-L_z/2,L_z/2} = 0$ and $\partial\psi/\partial z|_{z=-L_z/2,L_z/2} = 0$, and adiabatic (no flux) temperature boundary conditions are used. The direct numerical simulations are based on a compact fourth-order finite-difference scheme, proposed by Liu *et al.* [41], and the accuracy, stability, and efficiency of the scheme have been examined in great detail [41,42]. Recently, we have applied the same numerical code to study, respectively, small-scale properties in the 2D RT system [40] and turbulent heat transport in 2D Rayleigh-Bénard convection [43]. In the present study, the number of grid points is set to 4096×8193 in all the runs to achieve a sub-Kolmogorov-scale resolution.

The initial condition in our simulations is that the velocity is zero everywhere $\mathbf{u}(\mathbf{x},t=0)=0$, and the temperature varies as a step function of the vertical coordinate z, $\theta(\mathbf{x},t=0) = -\mathrm{sgn}(z)\Theta_0/2$, with Θ_0 being the initial temperature jump that defines the Atwood number as $A = \beta\Theta_0/2$. RT instability is seeded by perturbing the initial condition with respect to the step profile. The interface $\theta=0$ is perturbed by a superposition of cosine waves, $\cos(2\pi kx/L_x+\phi_k)$, with $30\leqslant k\leqslant 60$, equal amplitude, and random phases ϕ_k [30,44]. To check the independence of the turbulent state from initial conditions, we have also perturbed the initial condition by adding 10% of white noise to the value of $\theta(x,z=0,t=0)$. The obtained results suggest the robustness of the present results. A total of 32 independent realizations have been produced by generating different perturbed interfaces and all statistical quantities studied in this paper are obtained by first calculating for each individual simulation and then averaging over all these realizations. In all the runs, $Ag = 0.25$, $L_z = 1$, $\Theta_0 = 1$, $\nu = \kappa = 2.89\times 10^{-6}$, corresponding to the Prandtl number $\mathrm{Pr} = \nu/\kappa = 1$. Simulations with the same parameters but a lower resolution 2048×4097 have also been carried out. Comparison between the two resolutions also suggests the robustness of the results presented here.

III. RESULTS AND DISCUSSION

First of all, we study the growth of the mixing zone. We define here the width of the mixing zone $h(t)$ as a z zone where $-0.4\Theta_0 \leqslant \langle\theta(\mathbf{x},t)\rangle_x \leqslant 0.4\Theta_0$ with $\langle\theta(\mathbf{x},t)\rangle_x$ being the mean vertical temperature profiles and $\langle\cdot\rangle_x$ a horizontal average. This threshold-based definition has been widely used in previous works [31]. The measured mixing zone width $h(t)$ is plotted as a function of t/τ in Fig. 1, where $\tau = \sqrt{L_z/Ag}$ is the characteristic time of the RT evolution. The dashed line in the figure marks the self-similar prediction of the t^2 growth law [23,24]. It is seen clearly that in the range $1.6\lesssim t/\tau\lesssim 4$ two types of lines collapse roughly on top of each other, indicating a quadratic growth of $h(t)$. Further studies show that the power spectra (not shown here) of both the velocity and temperature files obtained within the self-similar range cover a broad range of scales [40], indicating that a turbulent state has been well developed. Therefore, we shall later analyze the temporal evolution of $Q(\eta)$ within this time range. In the insets of Fig. 1, we display two snapshots of the temperature field obtained at the two ends of this time range, i.e., $t/\tau = 1.6$ and 4, and one sees that large-scale turbulent structures (plumes or spikes) dominate the flows within the self-similar regime of $h(t)$.

To see whether or not the present resolution can resolve the sub-Kolmogorov-scale statistics, we examine in Fig. 2(a) the temporal evolution of the Kolmogorov scale $\eta_K(t)$, normalized by the computational grid spacing Δ_g. Two features of the graph are worth noting. First, $\eta_K > 3\Delta_g$ for all the simulation times (see the horizontal dash-dot line) and η_K is even larger than $4\Delta_g$ at the late stage of the evolution. This guarantees the adequate resolution for small-scale turbulent structures. Secondly, within the self-similarity regime $1.6\lesssim t/\tau\lesssim 4$, η_K increases slightly with the temporal evolution. The dashed line in the figure indicates the dimensional scaling $t^{1/8}$ for reference, which describes well the temporal behavior of $\eta_K(t)$. This is inconsistent with previous theoretical predictions [36] and numerical results [40].

The adequacy of the numerical resolution adopted in our simulations can also be checked from the behavior of longitudinal velocity structure functions, $S_{2n}(\ell) = \langle(\delta_\ell v)^{2n}\rangle$, as the spatial separation ℓ approaches the smallest value allowed in the simulation, i.e., the grid spacing Δ_g. In the limit of vanishing ℓ, it is expected from Taylor expansion of $S_{2n}(\ell)$ that $S_{2n}(\ell)\approx \ell^{2n}\langle(\partial v_i/\partial x_i)^{2n}\rangle \sim \ell^{2n}$. To recover this analytic behavior, a superfine resolution is required, particulary for high Reynolds numbers and large n (Schumacher, Sreenivasan, and Yakhot, 2007 [46]). Figure 2(b) shows the longitudinal structure functions of the horizontal velocity u, for increasing orders n, from $n=1$ to 5, obtained at a late stage $t/\tau = 4$ of the self-similarity regime. The structure functions have been divided by ℓ^{2n} such that the analytic behavior can be indicated by asymptotic plateaus corresponding to $\langle(\partial u/\partial x)^{2n}\rangle$ (shown by horizontal dashed lines) for small enough ℓ. As expected, $S_{2n}(\ell)/\ell^{2n}\approx$ const. holds approximately in the dissipative range up to $n=5$.

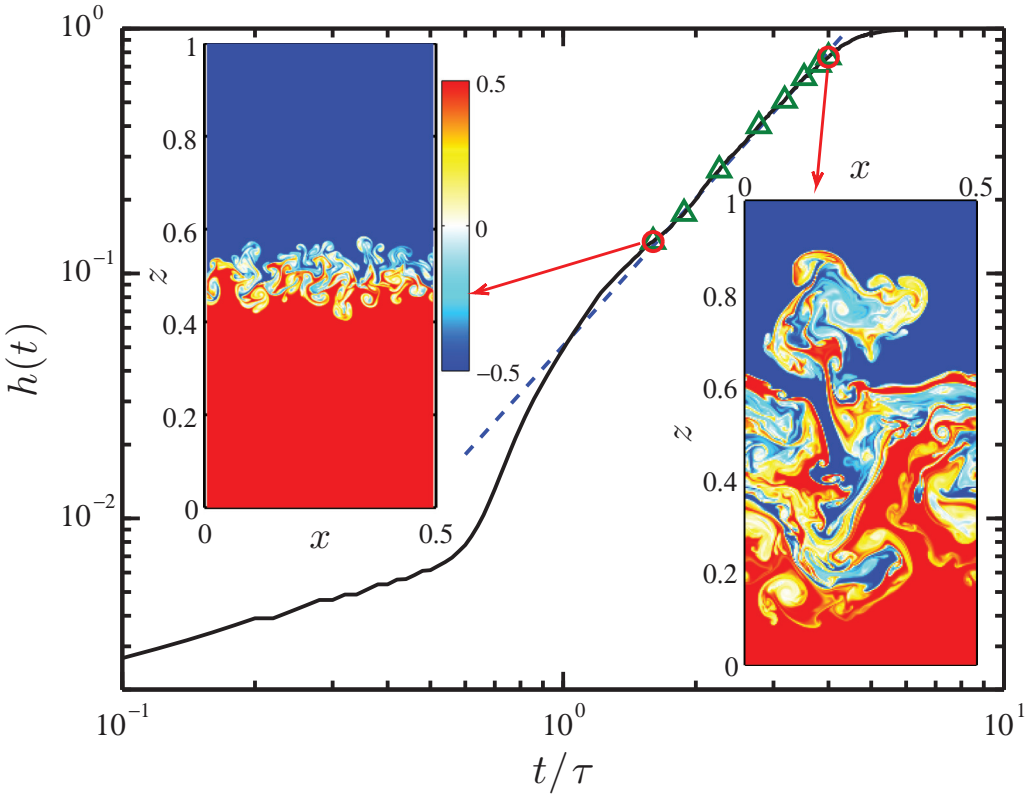

FIG. 1. (Color) The temporal evolution of the mixing layer width $h(t)$. The blue dashed line indicates the quadratic law $h(t) = \alpha A g t^2$ with $\alpha = 0.05$ obtained from the compensated plot of $h(t)/(Agt^2)$ (not shown here) for reference. Two snapshots of the temperature fields are shown at $t/\tau = 1.6$ (top left inset) and $t/\tau = 4$ (bottom right inset). Red and blue areas identify hot and cold regions, respectively. The dark-green triangles indicate the times of the eight examined fields in Fig. 6. The corresponding movie about the temporal evolution of the fields of the temperature, kinetic energy, and energy dissipation rate can be found in the Supplemental Material [45].

Figure 3 shows the normalized dissipation spectra, $2\nu k^2 E_u(k)/\epsilon_\theta^{2/5}$ [47], measured at $\mathrm{Re}_L = 370$, 1100, 3200, and 6500, respectively, corresponding to $t/\tau = 1.6$, 2.26, 3.18, and 4 in the self-similar regime of the RT evolution. Here, $\epsilon_\theta(t) \equiv \langle \kappa[\partial_i \theta(x,z,t)]^2 \rangle_V$ is the thermal dissipation rate where $\langle \cdots \rangle_V$ means a volume average inside the mixing zone, and $E_u(k)$ is the kinetic energy spectrum, which is calculated by fast Fourier transforming of the velocity fields on one-dimensional horizontal planes and then averaging over different z inside the mixing zone. Note that the expression $2\nu k^2 E_u(k)/\epsilon_\theta^{2/5}$ is applicable only at small scales where the field is expected to be isotropic. Nevertheless, we adopt this expression here since it has been widely used in previous studies [47]. One sees that in the intermediate range of k, corresponding to inertial scales, all these spectra collapse almost perfectly on top of each other, while the evolution of the spectra at small wave numbers reflects the growth of the integral length scale, a dynamical quantity representing the typical size of the large-scale turbulent eddies.

Let's now turn to distributions of η, $Q(\eta)$. The PDF $Q(\eta)$ is calculated from the simulation data in the following way. For a given time t in the self-similarity regime of the RT evolution, we first fix a length ℓ that is an integral multiple of the grid spacing Δ_g, i.e., $\ell = m\Delta_g$. The longitudinal velocity increments across the separation ℓ, $\delta_\ell v$, are then calculated at each grid site within the mixing zone. If the obtained value of $\ell|\delta_\ell v|/\nu$ is between 0.9 and 2 [11], it contributes to the occurrence of local dissipation at a scale $\ell = \eta$. $Q(\eta)$ is then computed as $Q(\eta) = qn(\eta)/N(\eta)$, where $N(\eta)$ is the total number of the calculated velocity increments over a separation η, $n(\eta)$ is the count of events among $N(\eta)$ that satisfy the local balance at scale η, and q is a normalization parameter determined from $\int Q(\eta)d\eta = 1$. This calculating approach is identical to those described in previous numerical [12] and experimental [13,15] studies. For the present 2D RT flows, either horizontal, $\delta_\ell u = u(x+\ell,z,t) - u(x,z,t)$, or vertical, $\delta_\ell w = w(x,z+\ell,t) - w(x,z,t)$, longitudinal velocity increments can be used to obtain $Q(\eta)$, denoted as $Q(\eta_x)$ and $Q(\eta_z)$, respectively.

The local dissipation scale η is usually rescaled by the scale η_0 [12] that can be evaluated as follows. According to the theory of Refs. [48] and [7], the matching scale between the dissipative and inertial parts of $S_{2n}(\ell)$, η_{2n}, is order dependent and can be give by

$$\eta_{2n} = L\mathrm{Re}_L^{\frac{1}{(\zeta_{2n}-\zeta_{2n+1}-1)}}, \tag{5}$$

where ζ_{2n} are the scaling exponents of $S_{2n}(\ell)$ in the inertial range, and $\mathrm{Re}_L = v'L/\nu$ is the integral-length-scale-based Reynolds number, with $v' = \sqrt{\langle (u - \langle u \rangle)^2 \rangle + \langle (w - \langle w \rangle)^2 \rangle}$. In 2D RT turbulence, as revealed by previous numerical studies [38–40], the statistics of velocity differences obeys the BO59 scaling and is nearly self-similar, i.e., $\zeta_{2n} = 6n/5$,

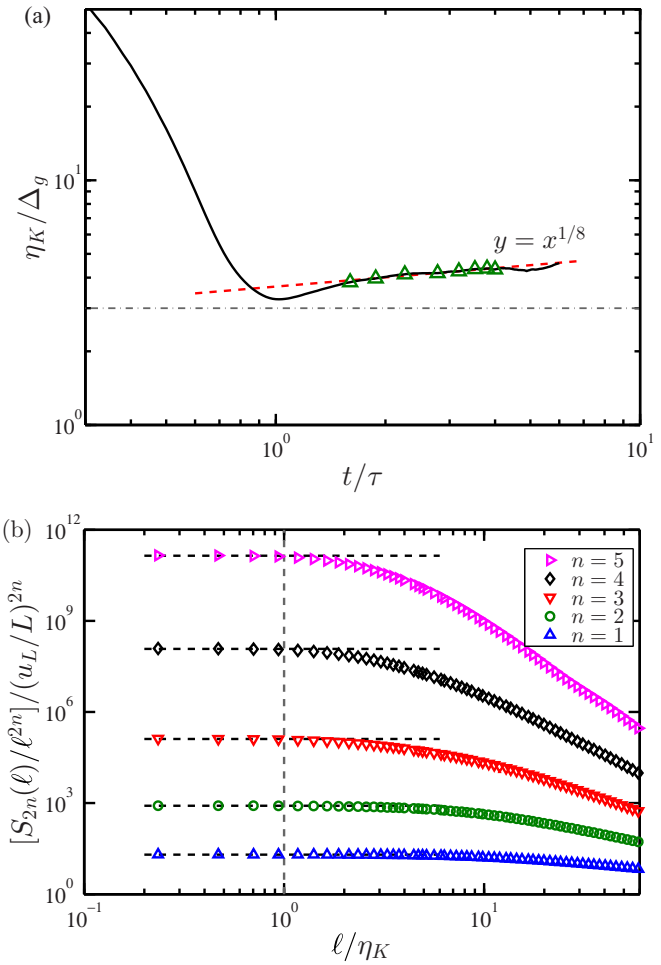

FIG. 2. (Color online) (a) The temporal evolution of the Kolmogorov scale $\eta_K(t)$, normalized by the computational grid spacing Δ_g. The red dashed line marks the dimensional scaling $t^{1/8}$ and the horizontal dash-dot line indicates the value of 3 for reference. The dark-green triangle symbols indicate the times of the eight examined fields in Fig. 6. (b) Test of analyticity for the compensated longitudinal velocity structure functions $S_{2n}(\ell)/\ell^{2n}$, normalized by $(u_L/L)^{2n}$, for $n = 1, 2, 3, 4$, and 5, obtained within the mixing zone and at $t/\tau = 4$ and $\mathrm{Re}_L = 6500$. Here, $u_L = \langle \delta_L u^2 \rangle^{1/2}$ is the typical velocity over the integral scale L. Horizontal dashed lines show the exact analytical form, corresponding to $S_{2n}(\ell)/\ell^{2n} = \text{const.}$, and the vertical dashed line indicates the Kolmogorov scale $\ell/\eta_K = 1$.

at least for orders $n \leq 5$. Inserting this into (5) yields

$$\eta_{2n} = L\mathrm{Re}_L^{-5/8} = \eta_K, \tag{6}$$

for 2D RT turbulence. Therefore, the relation,

$$\eta_0 = \eta_K = L\mathrm{Re}_L^{-5/8}, \tag{7}$$

is used to determine the value of η_0 in the present study. Equation (7) is a natural accompaniment of the BO59 scenario and it is different from the situations in other types of flows, such as homogeneous isotropic turbulence and turbulent pipe flows, where $\eta_K = L\mathrm{Re}_L^{-3/4}$ and $\eta_0 = L\mathrm{Re}_L^{-0.72}$ are expected due to the K41 cascades and the intermittency correction. Note that the relation (7) for η_K can also be obtained from the point of view of the temporal evolution of the RT system. According

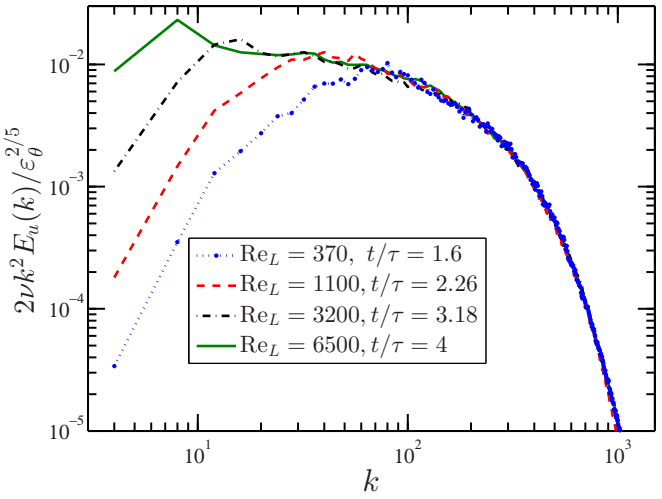

FIG. 3. (Color online) Dissipation spectra $2\nu k^2 E_u(k)$, compensated with $\epsilon_\theta^{2/5}$, measured at $\mathrm{Re}_L = 370$, 1100, 3200, and 6500, respectively, corresponding to $t/\tau = 1.6$, 2.26, 3.18, and 4.

to the phenomenological theory of 2D RT turbulence [36], the growth of the mixing zone width $h(t)$, a geometrical quantity, is accompanied by the growth of the integral scale $L(t)$, a dynamical quantity representing the characteristic scale of the production of turbulence, i.e.,

$$L(t) \sim h(t) \sim t^2, \tag{8}$$

which further implies

$$v'(t) \sim \frac{L(t)}{t} \sim t \ \text{ and } \ \mathrm{Re}_L(t) = \frac{v'(t)L(t)}{\nu} \sim t^3. \tag{9}$$

Temporal scalings (8) and (9) have been numerically validated [40] and combining these and the scaling $\eta_K \sim t^{1/8}$ from Fig. 2(a) can recover the relation (7).

In Fig. 4(a), direct comparison is made between $Q(\eta_x/\eta_0)$ (open circles) and $Q(\eta_z/\eta_0)$ (solid triangles) for three different Reynolds numbers, $\mathrm{Re}_L = 610$, 3200, and 6500, which are obtained within the self-similarity regime of the RT evolution. It is seen that at each Reynolds number, distributions obtained in horizontal and vertical directions are almost identical to each other within nearly all the studied scales. To see this more clearly, we plot in Fig. 4(b) the corresponding ratios between $Q(\eta_x)$ and $Q(\eta_z)$. For clarity, the $\mathrm{Re}_L = 3200$ and 6500 data have been shifted upwards by the values of 1 and 2, respectively, with respect to the $\mathrm{Re}_L = 610$ data. Again one can see the growth of the integral length scale which is similar to that revealed by Fig. 3. One also sees that $Q(\eta_x)$ agrees excellently with $Q(\eta_z)$ for small scales. This suggests that the dynamics of turbulent dissipation at small scales is nearly isotropic in RT turbulence. As the present flow is driven by buoyancy in the vertical direction and previous studies have shown that the forcing due to gravity induces anisotropy to the flow at large scales [40], the results shown in Fig. 4 reveal that at small scales distributions of η_x and η_z for velocity components along different directions are insensitive to such buoyancy-induced large-scale anisotropy. For large scales, however, it is seen in Fig. 4(b) that $Q(\eta_x)$ is a little larger

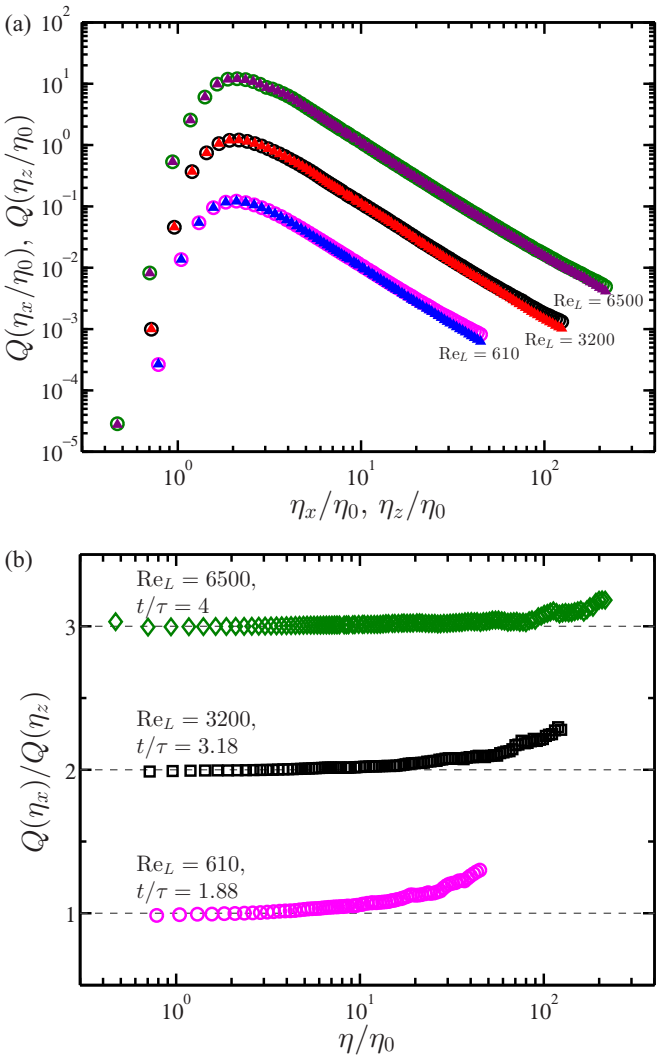

FIG. 4. (Color online) (a) The measured PDFs of the local dissipation scales for the horizontal and vertical velocity components, $Q(\eta_x/\eta_0)$ (open circles) and $Q(\eta_z/\eta_0)$ (solid triangles), for $\mathrm{Re}_L = 610$, 3200, and 6500 (corresponding to $t/\tau = 1.88$, 3.18, and 4, respectively). For clarity, the $\mathrm{Re}_L = 3200$ and 6500 data have been shifted upwards by one and two decades, respectively, with respect to the $\mathrm{Re}_L = 610$ data. (b) The corresponding ratio between $Q(\eta_z)$ and $Q(\eta_z)$. For clarity, the $\mathrm{Re}_L = 3200$ and 6500 data have been shifted upwards by the values of 1 and 2, respectively, with respect to the $\mathrm{Re}_L = 610$ data.

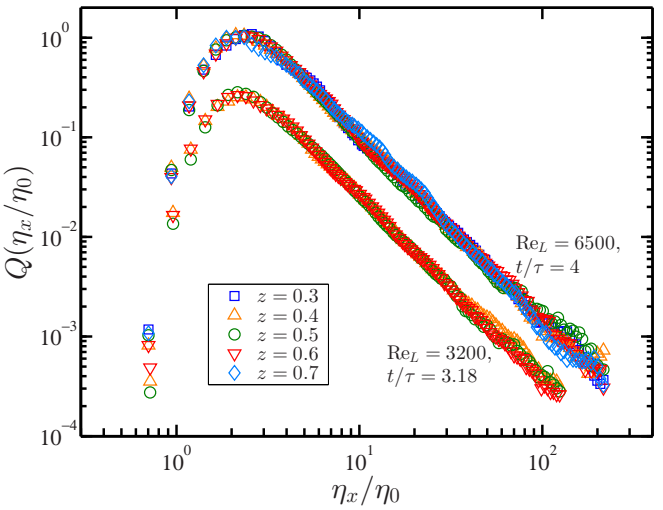

FIG. 5. (Color online) PDFs of the local dissipation scales, $Q(\eta_x)$, for horizontal velocity components obtained at different vertical positions z for $\mathrm{Re}_L = 3200$ and 6500 (corresponding to $t/\tau = 3.18$ and 4, respectively). To acquire accurate statistics, $Q(\eta_x)$ for each z was calculated within a horizontal layer of width $0.0025L_z$ around z. For clarity, the $\mathrm{Re}_L = 6500$ data have been shifted upwards by a value of 4 with respect to the $\mathrm{Re}_L = 3200$ data.

than $Q(\eta_z)$, which may be a manifestation of the large-scale anisotropy.

Some recent works have shown that in turbulent passive and active scalar mixing fields, the flow structure across the interface shows on one side to be highly influenced by the outer environment of the evolution [49], and on the other side to contain two layers of high intermittency aside the initial interface [50]. To reveal the former effect requires performing additional simulations while changing the outer environments and this will be the objectives of our future studies. For the latter effect, we examined the PDFs of the dissipation scales in horizontal planes at different vertical positions z. Figure 5 shows $Q(\eta_x)$ measured at different z for $\mathrm{Re}_L = 3200$ and 6500. To acquire accurate statistics, $Q(\eta_x)$ for each z was calculated within a horizontal layer of width $0.0025L_z$ around z. [Note that $0.0025L_z$ corresponds to $0.0049h(t)$ and $0.0033h(t)$ for the $\mathrm{Re}_L = 3200$ and 6500 data, respectively.] For clarity, the $\mathrm{Re}_L = 6500$ data have been shifted upwards by a value of 4 with respect to the $\mathrm{Re}_L = 3200$ data. One sees that for either data set $Q(\eta_x)$ obtained at different z collapse roughly on top of each other, although the distributions seem to scatter a little, which may be due to the limited statistics. This suggests that the distribution of the local dissipation scales is position independent.

Figure 6 shows $Q(\eta/\eta_0)$ obtained at eight different evolution times in the self-similarity regime, corresponding to Re_L varying from 370 to 6500. Here, $Q(\eta/\eta_0)$ was computed by averaging over both horizontal and vertical directions of separations. Excellent collapse of $Q(\eta/\eta_0)$ can be seen for all studied Reynolds numbers, suggesting that distributions of η are independent of the mixing zone evolution. Note that the numerical data from homogeneous isotropic box turbulence [12] showed that the left tail of $Q(\eta)$ exhibits a slight Reynolds number dependence, which indicates an increasing probability that very fine sub-Kolmogorov scales will appear. However, in the present study we do not observe such a weak Reynolds number dependence for small η.

For comparison, we also plot in Fig. 6 the numerical results from homogeneous isotropic box turbulence at Taylor-microscale Reynolds number $\mathrm{Re}_\lambda = 151$ [12] (solid line) and the experimental results measured in the anisotropic log layer of turbulent pipe flows at $\mathrm{Re}_\lambda = 155$ [11]. It is seen that there is a very good agreement between the present and previous results, at least for the smallest scales around the classical Kolmogorov dissipation scale. This result is somewhat unexpected and surprising, as the phenomenology of 2D RT turbulence is completely different from that of

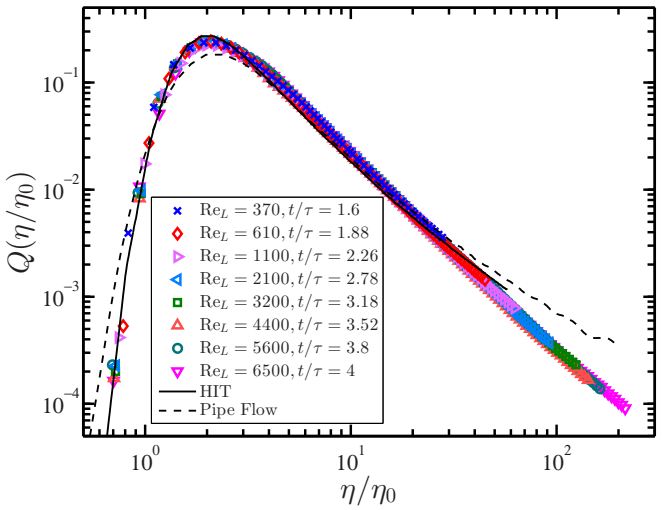

FIG. 6. (Color online) The measured PDFs of the local dissipation scales $Q(\eta/\eta_0)$ for $\mathrm{Re}_L = 370$, 610, 1100, 2100, 3200, 4400, 5600, and 6500. Here, $Q(\eta/\eta_0)$ was computed by averaging over both horizontal and vertical directions of separations. For comparison, numerical results from homogeneous isotropic turbulence (HIT) at Taylor-microscale Reynolds number $\mathrm{Re}_\lambda = 151$ [12] (solid line) and experimental results measured in the anisotropic log layer of turbulent pipe flows at $\mathrm{Re}_\lambda = 155$ [11] (dashed line) are also shown. (The two data sets were both taken from Fig. 4 of Ref. [11] using data capturing software.)

3D turbulence. While in 3D turbulence the fluctuations of dissipation scale η are due to the intermittent nature of the cascade process which transfers the energy from the large injection scales toward the small dissipative scales, in 2D RT turbulence the transfer of kinetic energy is reversed, i.e., it proceeds from small scales toward the large-scale structures of the flow. Therefore, the results shown in Fig. 6 suggest that the dynamics of turbulent dissipation at the smallest scales is insensitive to the details of the flows at large scales, as well as to the cascade process of kinetic energy. We further notice that the agreement between the present and previous results is not so good for large scales $\eta/\eta_0 \gtrsim 30$, i.e., the RT case seems to show a different trend from the other two cases. As the shape of the right tail of $Q(\eta)$ is dominated by the inertial-range intermittency [13], the observed disagreement in the right tails may be due to the lack of the inertial-range intermittency for the velocity field in 2D RT turbulence [40].

IV. CONCLUSION

To conclude, we have performed a very careful investigation of distributions of the local dissipation scale η, $Q(\eta)$, in RT turbulence in two dimensions, by means of direct numerical simulations. We present results from an ensemble of 32 independent realizations carried out at small Atwood number and unit Prandtl number with a spatial resolution of 4096×8193 grid points that can resolve the sub-Kolmogorov-scale statistics. Our results show that at small scales $Q(\eta)$ is insensitive to the large-scale anisotropy of the flow induced by the forcing due to gravity. This result is not surprising, since the system's energy (information) is transferred from small scales to large scales, the opposite direction for dissipation-related scale η. The measured $Q(\eta)$ is also found to be independent of position and of the mixing zone evolution. Comparison between the present results and those obtained previously in homogeneous isotropic box turbulence [12] and turbulent pipe flows [11] shows that the three data sets agree with each other at the smallest scales around the classical Kolmogorov dissipation scale. However, the RT case seems to show a different trend from the other two cases for large scales, which may be attributed to the absence of the inertial-range intermittency for the velocity field in 2D RT turbulence.

ACKNOWLEDGMENTS

This work was supported by Natural Science Foundation of China under Grants No. 11102114, No. 11222222, No. 11332006, and No. 11161160554, Innovation Program of Shanghai Municipal Education Commission under Grants No. 13YZ008 and No. 13YZ124, Shanghai Shuguang Project under Grant No. 13SG40, and Program for New Century Excellent Talents in University under Grant No. NCET-13. Q.Z. wishes to acknowledge support given to him from the organization department of the CPC central committee through National Program for Support of Top-notch Young Professionals.

[1] A. N. Kolmogorov, Dokl. Akad. Nauk SSSR **30**, 290 (1941).
[2] U. Frisch, *Turbulence* (Cambridge University Press, Cambridge, 1995).
[3] K. R. Sreenivasan and R. A. Antonia, Annu. Rev. Fluid Mech. **29**, 435 (1997).
[4] T. Ishihara, T. Gotoh, and Y. Kaneda, Annu. Rev. Fluid Mech. **41**, 165 (2009).
[5] B. W. Zeff, D. D. Lanterman, R. McAllister, R. Roy, E. J. Kostelich, and D. P. Lathrop, Nature (London) **421**, 146 (2003).
[6] J. M. Wallace and P. V. Vukoslavcević, Annu. Rev. Fluid Mech. **42**, 157 (2010).
[7] V. Yakhot, Physica D **215**, 166 (2006).
[8] V. Yakhot, J. Fluid Mech. **606**, 325 (2008).
[9] V. Yakhot and K. R. Sreenivasan, J. Stat. Phys. **121**, 823 (2005).
[10] L. Biferale, Phys. Fluids **20**, 031703 (2008).
[11] S. C. C. Bailey, M. Hultmark, J. Schumacher, V. Yakhot, and A. J. Smits, Phys. Rev. Lett. **103**, 014502 (2009).
[12] J. Schumacher, Europhys. Lett. **80**, 54001 (2007).
[13] Q. Zhou and K.-Q. Xia, Phys. Rev. Lett. **104**, 124301 (2010).
[14] P. E. Hamlington, D. Krasnov, T. Boeck, and J. Schumacher, J. Fluid Mech. **701**, 419 (2012).
[15] K. N. Morshed, S. K. Venayagamoorthy, and L. P. Dasi, Phys. Fluids **25**, 011701 (2013).
[16] L. Rayleigh, Proc. R. Math. Soc. **14**, 170 (1883).
[17] G. I. Taylor, Proc. R. Soc. London A **201**, 192 (1950).

[18] D. M. Schultz, K. M. Kanak, J. M. Straka, R. J. Trapp, B. A. Gordon, D. S. Zrnic, G. H. Bryan, A. J. Durant, T. J. Garrett, P. M. Klein *et al.*, J. Atmos. Sci. **63**, 2409 (2006).
[19] H. Isobe, T. Miyagoshi, K. Shibata, and T. Yokoyama, Nature (London) **434**, 478 (2005).
[20] J. J. Tao, X. T. He, W. H. Ye, and F. H. Busse, Phys. Rev. E **87**, 013001 (2013).
[21] R. P. Taleyarkhan, C. D. West, J. S. Cho, R. T. L., Jr., R. I. Nigmatulin, and R. C. Block, Science **295**, 1868 (2002).
[22] M. Zingale, S. E. Woosley, C. A. Rendleman, M. S. Day, and J. B. Bell, Astrophys. J. **632**, 1021 (2005).
[23] W. H. Cabot and A. W. Cool, Nat. Phys. **2**, 562 (2006).
[24] G. Dimonte, D. L. Youngs, A. Dimits, S. Weber, M. Marinak, S. Wunsch, C. Garasi, A. Robinson, M. J. Andrews, P. Ramaprabhu *et al.*, Phys. Fluids **16**, 1668 (2004).
[25] S. I. Abarzhi, Phil. Trans. R. Soc. A **368**, 1809 (2010).
[26] S. B. Dalziel, P. F. Linden, and D. L. Youngs, J. Fluid Mech. **399**, 1 (1999).
[27] Y. Zhou, Phys. Fluids **13**, 538 (2001).
[28] P. N. Wilson and M. J. Andrews, Phys. Fluids **14**, 938 (2002).
[29] T. Matsumoto, Phys. Rev. E **79**, 055301(R) (2009).
[30] G. Boffetta, A. Mazzino, S. Musacchio, and L. Vozella, Phys. Rev. E **79**, 065301(R) (2009).
[31] G. Boffetta, F. D. Lillo, A. Mazzino, and S. Musacchio, J. Fluid Mech. **690**, 426 (2012).
[32] N. Vladimirova and M. Chertkov, Phys. Fluids **21**, 015102 (2009).
[33] D. Chung and D. I. Pullin, J. Fluid Mech. **643**, 279 (2010).
[34] O. Soulard and J. Griffond, Phys. Fluids **24**, 025101 (2012).
[35] D. Lohse and K.-Q. Xia, Annu. Rev. Fluid Mech. **42**, 335 (2010).
[36] M. Chertkov, Phys. Rev. Lett. **91**, 115001 (2003).
[37] O. Soulard, Phys. Rev. Lett. **109**, 254501 (2012).
[38] A. Celani, A. Mazzino, and L. Vozella, Phys. Rev. Lett. **96**, 134504 (2006).
[39] L. Biferale, F. Mantovani, M. Sbragaglia, A. Scagliarini, F. Toschi, and R. Tripiccione, Phys. Fluids **22**, 115112 (2010).
[40] Q. Zhou, Phys. Fluids **25**, 085107 (2013).
[41] J.-G. Liu, C. Wang, and H. Johnston, J. Sci. Comput. **18**, 253 (2003).
[42] W. E and J.-G. Liu, J. Comput. Phys. **124**, 368 (1996).
[43] Y.-X. Huang and Q. Zhou, J. Fluid Mech. **737**, R3 (2013).
[44] T. T. Clark, Phys. Fluids **15**, 2413 (2003).
[45] See Supplemental Material at http://link.aps.org/supplemental/10.1103/PhysRevE.90.043012 for movie about the temporal evolution of the fields of the temperature, kinetic energy, and energy dissipation rate.
[46] J. Schumacher, K. R. Sreenivasan, and V. Yakhot, New J. Phys. **9**, 89 (2007).
[47] S.B. Pope, *Turbulent Flows* (Cambridge University Press, Cambridge, 2000).
[48] V. Yakhot and K. R. Sreenivasan, Physsica A **343**, 147 (2004).
[49] P. Ripesi, L. Biferale, S. F. Schifano, and R. Tripiccione, Phys. Rev. E **89**, 043022 (2014).
[50] M. Iovieno, S. D. Savino, L. Gallana, and D. Tordella, J. Turbulence **15**, 311 (2014).